TECHNISCHE UNIVERSITÄT CHEMNITZ

Sonderforschungsbereich 393

Parallele Numerische Simulation für Physik und Kontinuumsmechanik

Arnd Meyer, Frank Rabold, Matthias Scherzer

Efficient Finite Element Simulation of Crack Propagation

Preprint SFB393/04-01

Abstract

The preprint delivers an efficient solution technique for the numerical simulation of crack propagation of 2D linear elastic formulations based on finite elements together with the conjugate gradient method in order to solve the corresponding linear equation systems. The developed iterative numerical approach using hierarchical preconditioners comprehends the interesting feature that the hierarchical data structure will not be destroyed during crack propagation. Thus, one gets the possibility to simulate crack advance in a very effective numerical manner including adaptive mesh refinement and mesh coarsening. Test examples are presented to illustrate the efficiency of the given approach. Numerical simulations of crack propagation are compared with experimental data.

Preprintreihe des Chemnitzer SFB 393

ISSN 1619-7178 (Print) ISSN 1619-7186 (Internet)

SFB393/04-01 Februar 2004

Contents

Author's addresses:

Arnd Meyer
TU Chemnitz
Fakultät für Mathematik

D-09107 Chemnitz

Matthias Scherzer, Frank Rabold
TU Bergakademie Freiberg
Fakultät für Maschinenbau, Verfahrens- und Energietechnik
D-09596 Freiberg

http://www.tu-chemnitz.de/sfb393/

1 Introduction

Fracture of materials and several components of high technology engineering displays one of the central problems in modern strength analyzes. Today, fracture mechanics forms an autonomous research area of solid mechanics in order to explain phenomena of fracture, fatigue, and strength of materials for development of materials which are better failure-resistant than the conventional materials and to develop design methods that are better failure-safe than the conventional ones. Although, the entire fracture mechanics approaches cannot altogether be ascribed to crack type problems, the consideration and examination of the essential conditions leading to crack propagation, crack deflection and crack arrest is of highly practical and theoretical interests. Generally, analytical solutions for most of these crack problems in finite body domains are not attainable. Thus, it is necessary to develop numerical techniques for strength analysis of cracked structures subjected to various kinds of loads.

Three well known numerical methods having the ability to solve crack propagation boundary value problems for finite body domains can be mentioned [35]:

- the Finite Element Method,
- the Boundary Element Method,
- the Meshless Galerkin Method.

The Finite Element Method (FEM) is used to solve crack and crack propagation problems for over 30 years. On the one hand, one can find nowadays a big number of publications concerning even dynamic crack growth as it follows from the papers [11, 24, 35] and the references therein as well as from the reviews [6, 25, 26]. On the other hand, crack propagation modeling still represents a complicated problem and different specific definitions of crack propagation are used in the literature.

- First, it is difficult to describe the changeover from a continuous solid medium having strong continuity requirements on the displacements and their derivatives to final displacement jumps with new free surfaces inside the solid. Generally, the modeling of this procedure should be based on continuum approaches [27] leading to well-posed boundary value problems including crack growth. For this purpose, one needs improved cohesive models following from the realized critical stress and deformation states surrounding the advancing crack tips, in general, for non-linear material behavior. It is well known that classical plastic inviscid material models containing strain softening lead to ill-posed problems, and thus, are not useful to model crack propagation. It's quite plain that the well-posedness of such formulations cannot be restored by means of numerical techniques. The problem formulations have to prevent ill-posedness in order to get stable solutions depending continuously on the initial parameters in connection with the application of stable numerics.

- Second, an essential technical effort is necessary to include the algorithmic extensions of the FEM technology for the crack advance procedures [20] if the constitutive definition of the fracture process (point one) is established. In this context, Belytschko and co-workers have worked out the extended Finite Element Method (X-FEM) [4, 5] by adding enrichment functions to the approximation containing discontinuities for the crack propagation. This method was already expanded to 3D crack propagation problems in [14, 23] and induced an essential progress in crack advance simulation.

- Third, the numerical solution procedure for the corresponding boundary value problem with changing boundaries has to be made as efficient as possible, otherwise more complicated, that is, more realistic crack growth assemblies are not practicable to calculate. Thus, it is necessary to have excellent solutions surrounding the tips, including the asymptotic behavior, where the fracture process occurs. Away from the cracks, the numerical solution does not require very high resolution. In fact, one needs adaptivity of the solution based on a posteriori error estimation [12, 28, 34] together with effective capable solvers for the discrete solution system at each step of crack propagation.

The Boundary Element Method (BEM), which reduces the dimensionality of the problem by one degree can be applied effectively to crack advance problems for linear elastic formulations. On the one hand, the large effort of remeshing during crack propagation is not necessary by means of BEM. On the other hand, BEM encounters difficulties in connection with artificial boundaries which must be introduced repeatedly for each increment of crack extension. The publications [1, 2] and the references therein can be used for more details about BEM-applications in crack advance problems.

Meshfree methods [18, 19, 21] were used in the past for numerical simulation of non-linear boundary value problems including elastic-plastic and strain localization problems. They do not need to generate a connectivity matrix and thus, they are especially suited for adaptive refinements and for discontinuous field problems or solutions with high gradients [16]. Meshless methods are capable to reproduce crack growth by means of special enrichments for the nodal shape functions [13, 37]. On the other hand, the main difficulties of these methods consist in the imposition of the essential boundary conditions [8] as well as in the complicated structure of the shape functions [9] leading to difficult integration procedures. Thus, it seems challenging to combine the advantages of the meshless methods with the advantages of FEM in order to achieve optimal solutions in the sense of efficiency and accuracy [16].

In this paper, we focus on efficient solution techniques for the numerical simulation of crack propagation in 2D linear elastic formulations based on FEM together with the conjugate gradient method (PCGM) solving the corresponding linear equation systems. The developed iterative numerical technique using hierarchical preconditioners comprehends the interesting feature that the hierarchical data structure will not be destroyed during crack propagation. Thus, one gets the possibility to simulate crack advance in a very effective

numerical manner including adaptive mesh refinement and mesh coarsening. Test examples are presented to illustrate the efficiency of the given approach.

2 Formulation of the Problem

Let us consider the governing equations of a linear two-dimensional boundary value problem for isotropic elasto-statics with an advancing crack as shown in Figure 1. The boundary of the studied region Ω is subdivided into the following parts: The displacements $\boldsymbol{u}^*$ are prescribed on S_u of the outer boundary $S{=}S_u \cup S_T$ and stress loads $\boldsymbol{T}^*$ are given on S_T. Throughout the paper, bold typed variables denote vectors and tensors of second degree in $\mathbb{R}^2$. Our considerations will be restricted to two-dimensional problems embedded in $\mathbb{R}^3$. In addition to S, the crack surfaces a^+ and a^- represent an additional boundary inside Ω together with the crack advance length scales Δa^+ and Δa^- ($\mid \Delta a^+ \mid = \mid \Delta a^- \mid$). The direction and the magnitude of Δa^+ follow from corresponding crack advance models used in fracture mechanics. Thus, the strong equilibrium equations and the boundary conditions have the form:

$$\boldsymbol{\nabla \cdot \sigma} = \boldsymbol{0} \text{ in } \Omega, \quad \boldsymbol{\sigma \cdot n} = \boldsymbol{T}^* \text{ on } S_T, \quad \boldsymbol{u} = \boldsymbol{u}^* \text{ on } S_u, \tag{2.1}$$

$$\boldsymbol{\sigma \cdot n} = \boldsymbol{0} \text{ on } a^+,\ a^-,\ \Delta a^+ \text{ and } \Delta a^-. \tag{2.2}$$

In (2.1) and (2.2) $\boldsymbol{\sigma}$, $\boldsymbol{u}$ and $\boldsymbol{n}$ denote the stress tensor, the displacement vector and the unit normal vector corresponding to the given surfaces, respectively. $\boldsymbol{\nabla}$ represents the Nabla operator which is defined through

$$\boldsymbol{\nabla} = \boldsymbol{e}^i \frac{\partial}{\partial x_i}. \tag{2.3}$$

Recurring indices mean the application of Einstein's summation convention. The vectors $\boldsymbol{e}^i$ (i=1,2) span the dual basis regarding $\boldsymbol{e}_i$ as shown in Figure 1 with respect to the coordinates x_i. The symbol $\cdot$ stands for the scalar (inner) product of two vectors.

Throughout our considerations, we will use the geometrically linear fashion of continuum mechanics, that is, the deformation tensor $\boldsymbol{\varepsilon}$ is related to the displacements $\boldsymbol{u}$ by means of

$$\boldsymbol{\varepsilon} = \boldsymbol{\varepsilon}(\boldsymbol{u}) = \frac{1}{2}\left(\boldsymbol{\nabla u} + (\boldsymbol{\nabla u})^T\right). \tag{2.4}$$

$(\boldsymbol{\nabla u})^T$ denotes the transpose of $\boldsymbol{\nabla u}$. To complete the description of the boundary value problem, the material equations relating $\boldsymbol{\sigma}$ to $\boldsymbol{\varepsilon}$ have to be established. They will be applied in the form of an isotropic elastic solid

$$\boldsymbol{\sigma} = \boldsymbol{C} : \boldsymbol{\varepsilon} = \lambda I_1(\boldsymbol{\varepsilon})\boldsymbol{I} + 2\mu\boldsymbol{\varepsilon} \tag{2.5}$$

for plane strain conditions ($\boldsymbol{u} = u^1(x_1, x_2)\boldsymbol{e}_1 + u^2(x_1, x_2)\boldsymbol{e}_2,\ u^3 = 0$). λ and μ denote Lame's coefficients, which follow from Young's Modulus E and Poisson's ratio ν by means of

$$\lambda = \frac{\nu E}{(1+\nu)(1-2\nu)},\ \mu = \frac{E}{2(1+\nu)}. \tag{2.6}$$

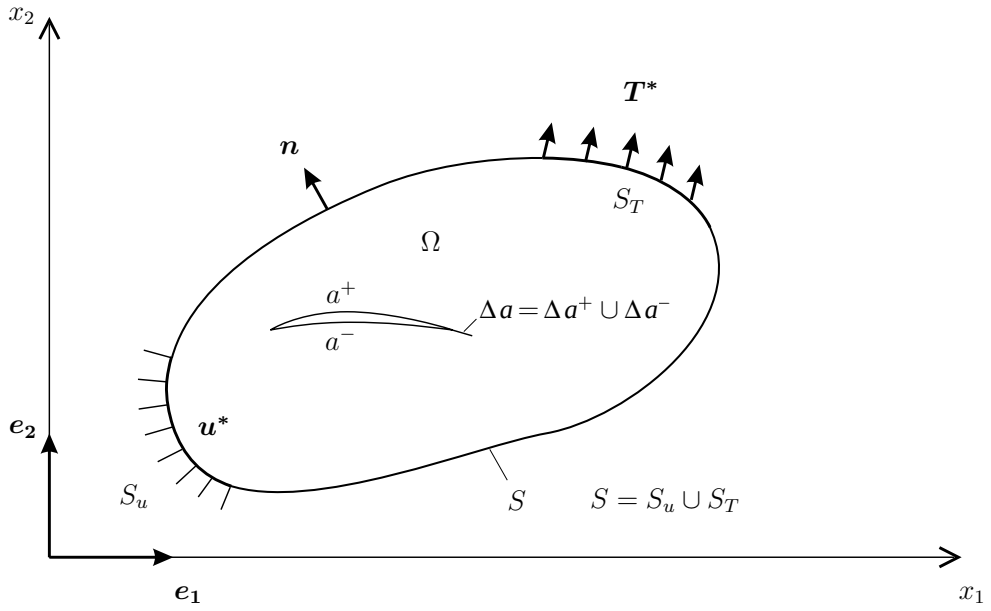

Figure 1: Two-dimensional elastic body domain with an advancing crack

$I_1(\boldsymbol{\varepsilon}) = \boldsymbol{\nabla}\cdot\boldsymbol{u}$ and $\boldsymbol{I} = \boldsymbol{e}_i\boldsymbol{e}^i = \boldsymbol{e}^i\boldsymbol{e}_i$ represent the first invariant of $\boldsymbol{\varepsilon}$ and the unit (metric) tensor of second degree, respectively. The symbol : means twice application of $\cdot$. So much about the strong formulation.

Solving problems for finite solids with real crack advance under arbitrary loads on the boundaries, these strong equations are not useful. Thus, instead of (2.1) to (2.5), the associated weak formulation($\boldsymbol{\sigma}\cdot\boldsymbol{n} = \boldsymbol{T}^*$ on S_T)

$$\iint_{\Omega} \boldsymbol{\varepsilon}(\boldsymbol{v}) : \boldsymbol{C} : \boldsymbol{\varepsilon}(\boldsymbol{u})\, d\Omega = \int_{S_T} \boldsymbol{v}\cdot\boldsymbol{T}^*\, dS,\ \forall \text{ test displacements } \boldsymbol{v}\ (\boldsymbol{v} = \boldsymbol{0} \text{ on } S_u) \tag{2.7}$$

will be applied. Making use of common finite element approximations for $\boldsymbol{u}$ and $\boldsymbol{v}$, the solution of the boundary value problem can be obtained for each specific crack length a. To model general crack propagation, it is necessary to write (2.7) in the incremental form for step by step loading based on the load increments $\Delta\boldsymbol{T}^* = \Delta\boldsymbol{\sigma}\cdot\boldsymbol{n}$ on S_T:

$$\iint_{\Omega} \boldsymbol{\varepsilon}(\boldsymbol{v}) : \boldsymbol{C} : \boldsymbol{\varepsilon}(\Delta\boldsymbol{u})\, d\Omega = \int_{S_T} \boldsymbol{v}\cdot\Delta\boldsymbol{T}^*\, dS - \int_{\Delta a} \boldsymbol{v}\cdot\boldsymbol{\sigma}^0\cdot\boldsymbol{n}\, dS,\ \forall\ \boldsymbol{v}\ (\boldsymbol{v} = \boldsymbol{0} \text{ on } S_u) \tag{2.8}$$

$\boldsymbol{\sigma}^0$ represents the calculated stresses of the previous load step at the current crack growth surface $\Delta a = \Delta a^+ \cup \Delta a^-$. The last integral in (2.8) defines the energy released during crack propagation along Δa. As assumed above, we will consider quasi-static problems, i.e., crack propagation displays a sequence of self-equilibrated steps. Thus, it is necessary to increment the load step by step and look for crack advance on the one hand. On the other hand, one can use the formulation (2.7) in the case of crack advance, instead of (2.8),

for the equilibrium at the end of the crack propagation step as a consequence of the linear quasi-static behavior. This circumstance simplifies the whole solution procedure and will be used in the following. At each load level, it is necessary to prove the critical crack advance conditions at the crack tips. If these conditions are fulfilled, the crack prolongates to $a+\Delta a$ and the solid gets the new surfaces Δa^+ and Δa^-. In continuum mechanics, the length scale Δa has to be assumed as an material parameter depending on the local stress state of the crack tip, and in general, on constitutive parameters influencing the fracture process [10]. Throughout the paper, we will suppose $|\Delta a^+|=|\Delta a^-|$ to be a given constant material parameter for simplicity.

The crack prolongation conditions are formulated in the classical way given, for instance, in [10] by means of two approaches. Based on the applied elastic material behavior, these conditions can be expressed through the two-dimensional J-integrals or through the corresponding stress intensity factors in an equivalent manner. The J-integral vector $\boldsymbol{J}$ is defined along Γ-contours surrounding the crack tip as shown in Figure 2 (the outer normals of these contours are labeled by $\boldsymbol{n}$ coinciding with the normal vector label on S).

$$\boldsymbol{J} = \int\limits_{\Gamma^-+\Gamma+\Gamma^+} \left((\tfrac{1}{2}\boldsymbol{\sigma} : \boldsymbol{\varepsilon})\boldsymbol{n} - \boldsymbol{\nabla u} \cdot \boldsymbol{\sigma} \cdot \boldsymbol{n} \right) ds \tag{2.9}$$

For the considered material behavior, $\boldsymbol{J}$ does not depend on the specific choice of the integration contour surrounding the crack tip. Thus, it characterizes the energy flux to the tip and renders possible the production of the new surfaces Δa in the case of crack advance with an extreme amount of power. The components of $\boldsymbol{J}$ with respect to the local xy-coordinate system at the crack tip are shown in Figure 2:

$$J_x = \boldsymbol{e}_x \cdot \boldsymbol{J}, \quad J_y = \boldsymbol{e}_y \cdot \boldsymbol{J}. \tag{2.10}$$

They are connected to the stress intensity factors K_I and K_{II} for the applied plane strain model by means of

$$J_x = \frac{1-\nu^2}{E}\left(K_I^2 + K_{II}^2\right), \quad J_y = -2\frac{1-\nu^2}{E} K_I K_{II}. \tag{2.11}$$

K_I and K_{II} provide the force criteria basis of fracture mechanics [17].

Applying the energetic approach [10], that is, the crack propagates along the direction of the J-integral vector $\mathbf{J}$ (Figure 2) if the magnitude $J = \sqrt{J_x^2 + J_y^2}$ of $\mathbf{J}$ reaches the critical value J_c ($J = J_c$), the frailure surface $F(K_I, K_{II}) = 0$ is defined through

$$F(K_I, K_{II}) = K_{Ic} - K_I \left((1+\rho^2)^2 + 4\rho^2 \right)^{\frac{1}{4}} = 0, \quad K_{Ic}^2 = \frac{J_c E}{1-\nu^2}, \ \rho = \frac{K_{II}}{K_I}. \tag{2.12}$$

K_{Ic} and ρ denote the fracture toughness and the ratio of K_{II} and K_I, respectively. For a standing crack, (2.12) defines crack advance Δa along the $\mathbf{J}$-direction with the angle θ (Figure 2):

$$\theta = \arctan \frac{-2\rho}{1+\rho^2}. \tag{2.13}$$

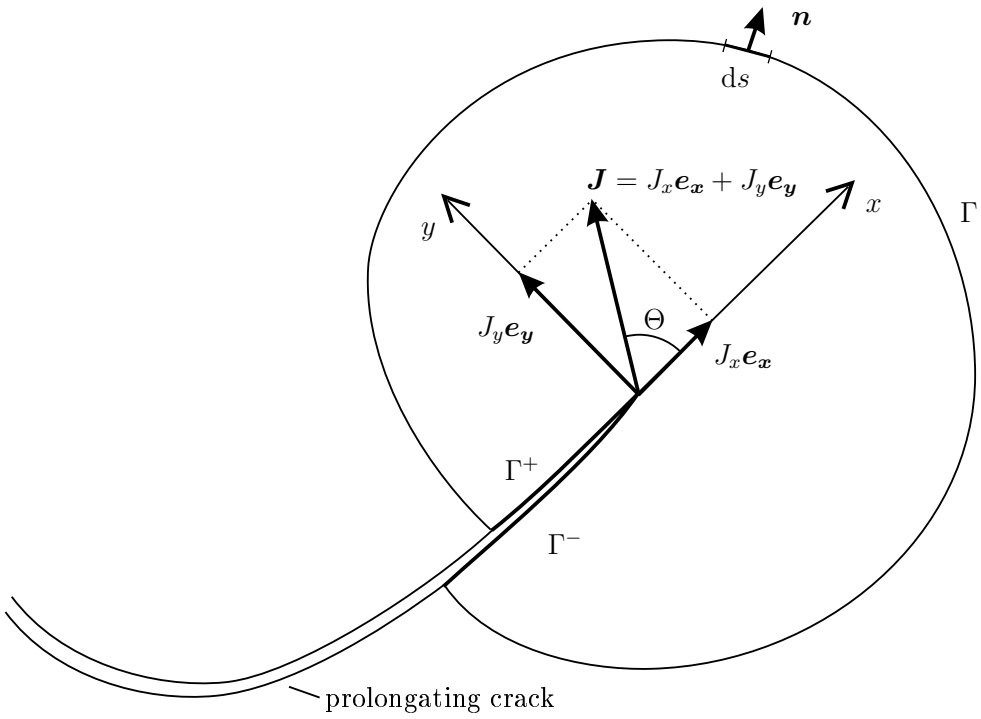

Figure 2: J-integral contour surrounding the crack tip

The second approach is based on the maximum hoop stress criteria. The crack will propagate perpendicular to the maximum circumferential stress plane if the corresponding stress intensity coefficient reaches K_{Ic} [10]. For this case, the crack direction θ_h and the failure surface $F_h(K_I, K_{II})$ result from

$$\theta_h = 2 \arctan \frac{1 - \sqrt{1 + 8\rho^2}}{4\rho}, \quad F_h(K_I, K_{II}) = K_{Ic} - K_I \frac{4\sqrt{2}\left(1 + 3\sqrt{1 + 8\rho^2}\right)(\mid \rho \mid)^3}{\left(12\rho^2 + 1 - \sqrt{1 + 8\rho^2}\right)^{3/2}} = 0. \tag{2.14}$$

Thus, the problem of crack growth in a two-dimensional isotropic elastic solid is formulated. The next section presents an efficient method for the necessary numerical solution.

3 Numerical solution based on efficient adaptive Finite Elements and iterative solver techniques

3.1 Adaptive Finite Element solution for fixed crack

The Finite Element simulation of the phenomenon described above requires some modern features, which are nowadays standard in scientific computing:

At first, the complicate structure of the solution around the crack tip (and its singularities) demand an adaptive mesh refinement. Although the position of the actual crack tip is known, we use an error controlled refinement procedure together with possible coarsening which is very attractive for later stages where the crack tip has moved on. Here, we apply locally the well–known residual error estimator [38] as error indicator on each existing finite element T

$$\eta_T^2 = \sum_{E \subset T} h_E \left\| [\boldsymbol{\sigma} \cdot \boldsymbol{n}] \right\|_{L_2(E)}^2 , \tag{3.1}$$

which measures the size of the stress jumps $[\boldsymbol{\sigma} \cdot \boldsymbol{n}]$ over the edges E of T. In the case of isotropic finite elements the weight h_E denotes the edge size divided by Young's modulus. Then,

$$\eta = \left(\sum_{\forall T} \eta_T^2 \right)^{1/2} \tag{3.2}$$

gives an approximation to the total $\mathbb{H}^1$–error size up to an unknown constant. Hence, for an element T with

$$\eta_T^2 > \alpha_{\text{refine}} \cdot \eta^2, \tag{3.3}$$

we should refine T and if

$$\eta_T^2 < \alpha_{\text{coarse}} \cdot \eta^2, \tag{3.4}$$

we should coarsen the mesh around T. (We choose $\alpha_{\text{refine}} \approx 0.8$ and reduce it up to 0.05 if not enough elements are refined and $\alpha_{\text{coarse}} = 10^{-3}$).

Second, this adaptive procedure requires a series of linear system solutions on each actual mesh, respectively. The finite element solutions on these meshes mainly have to guarantee that the error indicators are precise enough for a good mesh control in the refinement procedure.

Hence, we look for a very time efficient solution process enabling restricted accuracy on coarser meshes for domains away from cracks and crack tips. This is done with the help of the following ingredients:

- We store only the element matrices of each element T together with the element data. The assembly of any total stiffness matrix is not necessary. The solver, applying the preconditioned conjugate gradient method (PCGM), multiplies easily element by element. Thus, we can use the advantage only to generate element matrices on the new elements emerging from the refinement process. The elements away from cracks and crack tips do not need refinement and remain unchanged.

- The preconditioner uses the hierarchical data structure, which is contained in the history of subdividing the edges of the mesh. Such hierarchical data are necessary for all modern Multi–Level preconditioners such as the "Hierarchical Basis Preconditioner" (HB, see [39]), the BPX–preconditioner (see [7]) or all the well–known Multi-grid algorithms. For simulation in 2D, the most simple HB–preconditioner leads to a very quick solver, especially from the following reasons:

1. All information for implementing HB is contained in the "edge–subdivision–tree" from the mesh refinement used.
2. The number of arithmetic operations is about 3N for N unknowns in the actual mesh.
3. On the one hand, the condition number of the preconditioned stiffness matrix (equal to the condition number of the Finite Element stiffness matrix with respect to the hierarchical basis of the ansatz space) grows as $(\log N)^2$.
   On the other hand, we have a very good starting vector embedded into the adaptive loop on each new solution (only "high frequency error") leading to near constant number of iterations during the refinement.

We demonstrate the efficiency of the technique described above at a simple example with a crack of constant length ("slit–domain"). We start with a coarse mesh of 8 triangles (17 coarse edges, 10 nodes on vertices) for the domain

$$\Omega = (-1,1)^2 \setminus [0,1) \times \{0\}.$$

The node (1,0) occurs twice, as well as we have 2 distinct edges from (0,0) (the crack tip) to both nodes (1,0). The two adjacent triangles refer to the different edges. The coarse mesh solution shape and two finer solution shapes with about 1000 and 8000 nodes are presented in Figure 3.

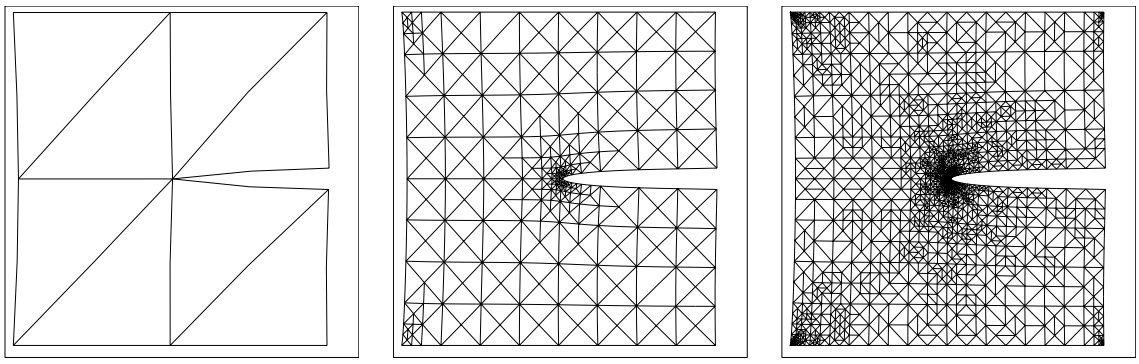

Figure 3: Mesh refinement on "Slit Domain" (here: prescribed displacements at bottom and top)

The following table contains some information about the adaptive refinement until 30 000 nodes. Each row belongs to one linear system solution with the times for generating the new elements and for the PCGM. Additionally, the number of elements to refine and to coarsen are given. Mainly, we watch the finite number of about 20 iterations on each mesh. The computations were realized by means of a Pentium IV with optimized FORTRAN. These very short running times are challenging for the moving crack situation. In fact, we should maintain most of the features described above, although the mesh connection will change in the case of an advancing crack.

Mesh -Info : #Nodes/#Elem's/ #Edges	Gener. time[s]	PCGM #It	PCGM time[s]	#Elements to ref/coars	est.Err. (square)
27 / 8 / 17	0.000	2	0.000	1 0	1.1E+01
85 / 32 / 75	0.001	14	0.001	3 0	5.2E+00
297 / 128 / 287	0.005	18	0.005	6 2	2.6E+00
643 / 254 / 633	0.008	20	0.011	10 84	3.5E+00
750 / 272 / 621	0.000	24	0.015	15 56	2.0E+00
1099 / 416 / 955	0.009	23	0.022	16 144	1.1E+00
1299 / 467 / 1040	0.006	24	0.027	24 115	6.2E-01
1702 / 626 / 1389	0.012	25	0.040	27 157	3.6E-01
		.			
		.			
		.			
		.			
6695 / 2822 / 6233	0.032	16	0.239	215 15	5.1E-03
8786 / 3803 / 8324	0.160	15	0.307	65 113	3.0E-03
9438 / 4088 / 8941	0.024	16	0.441	348 39	2.2E-03
12536 / 5534 / 12039	0.241	15	0.387	284 37	1.1E-03
15313 / 6845 / 14816	0.236	15	0.605	447 97	6.3E-04
19455 / 8747 / 18950	0.273	15	0.705	284 206	4.3E-04
22302 / 10088 / 21791	0.093	15	1.075	1059 93	3.0E-04
31961 / 14477 / 31450	0.574	15	1.451	230 820	2.0E-04

Table 1: The adaptive history: number of nodes, elements and edges, solver times and error estimators for quadratic triangular elements

3.2 Adaptive Finite Element solution for the crack propagation

If the refinement procedure of the previous section is applied until some small error criterion, we end up with a good Finite Element approximation of the true $\mathbb{H}^1$–solution belonging to any corresponding load level of the problem under consideration. The J–integrals introduced in Chapter 2 yield the propagation information of the crack movement.

Thus, we obtain the direction and the length $|\Delta a^+|=|\Delta a^-|$ defining the new crack tip. From this information, the segment L (straight line) from P (actual crack tip) to P_{new} (new crack tip) fixes the new crack surfaces which are to incorporate into the existing mesh as shown in Figure 4. In the usual manner of Finite Element routines, the new mesh opening can be calculated introducing nodes (hence edges of elements) along L with twice degrees of freedom. At node $\boldsymbol{x}$, we define $\boldsymbol{u}_+(\boldsymbol{x})$ and $\boldsymbol{u}_-(\boldsymbol{x})$ the displacements on both crack flanks. We call an element T a "–"-element if it contains "–"-degrees of freedom. "+"-elements belong to the other new crack flank and contain "+"-degrees of freedom, respectively.

The first step for the crack propagation modeling is the construction of these "–"- and "+"-elements by means of an (unusual) subdivision of all elements cutting L. Embedded into the adaptive mesh subdivision routine, this is done easily considering the edges E of the actual fine mesh and performing the following algorithm:

For each edge E do:

1. Calculate the intersection $\boldsymbol{Q}$ of L with E.
2. If no intersection: continue with next edge.
3. Let $E = (\boldsymbol{a}, \boldsymbol{b})$ with $\boldsymbol{a}, \boldsymbol{b} \in \mathbb{R}^2$ the end nodes, then $\boldsymbol{Q} = \alpha\, \boldsymbol{a} + (1 - \alpha)\, \boldsymbol{b}$.

   If α near 1 $\implies$ correct $\boldsymbol{a}$ to $\boldsymbol{Q}$ and continue with next edge.[1]
   If α near 0 $\implies$ correct $\boldsymbol{b}$ to $\boldsymbol{Q}$ and continue with next edge.

   Else: Subdivide the Edge E, producing $E_1 = (\boldsymbol{a}, \boldsymbol{Q})$ and $E_2 = (\boldsymbol{Q}, \boldsymbol{b})$.

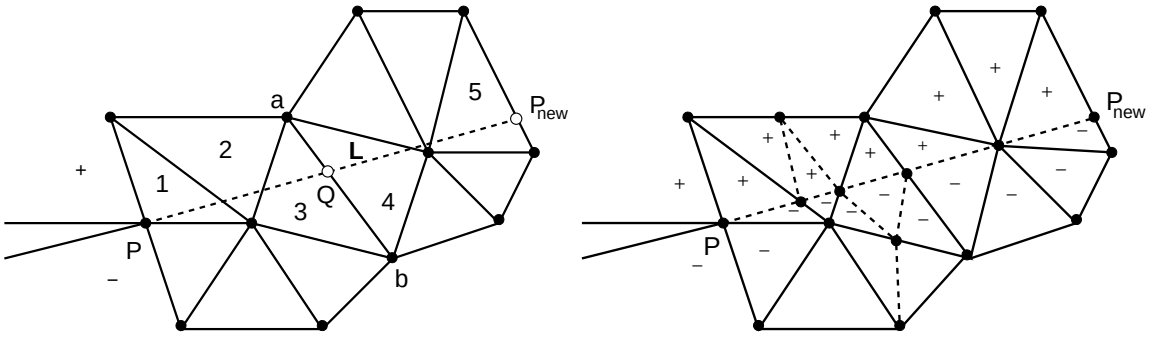

Figure 4: Mesh handling along section L, element 1 with "green", element 2 and 3 with "red" and 4,5 with "green" subdivision after node move

After this procedure, the usual mesh refinement routine subdivides all elements T surrounding L in "red" manner, if two adjacent edges of T are intersected by L. The other surrounding elements are subdivided "green", if they are intersected by L at one edge only. All other elements remain unchanged. This simple algorithm introduces the segment L as a couple of edges into our mesh. See Figure 4 for an example and Figure 5 for the explanation of "red" and "green" subdivision. This way, it is possible to define the "+" and "–" degrees of freedom at the new nodes along L.

In this context, we emphasize the important fact regarding the following efficient solver. Up to now, the hierarchical data structure is given within the subdivision tree of the edges. If we will double the edges along L this hierarchy will be destroyed and we cannot use an efficient hierarchical preconditioner anymore. Thus, we define only one edge, as it has been created from the algorithm above, which refers to the "–"-nodes. Each "–"-node has a copy as "+"-node in the nodal list and there is a reference from "–"-node to its "+"-partner

[1] These tests avoid very distorted elements.

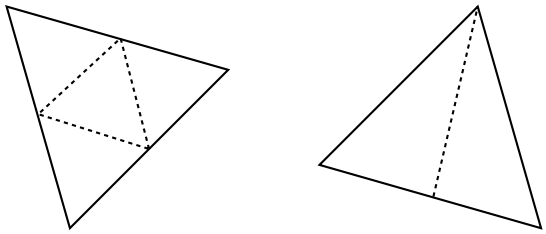

Figure 5: "red" (left) and "green" (right) subdivision

(and back) in the nodal list. Obviously, the "–"-elements refer to degrees of freedom of usual or "–"-nodes, the "+"-elements to such of usual or "+"-nodes.

In order to construct an efficient preconditioner we append the new unknowns first. By definition of "–"- and "+"-nodes we have:

n nodes with n usual nodal degrees of freedom [2]
d "–"-nodes with d nodal degrees of freedom and
d "+"-nodes with additionally d nodal degrees of freedom.

For this actual mesh, our linear system to solve has $N = n + d + d$ nodal degrees of freedom, but the hierarchical preconditioner C^{-1} available from the information of the edge tree acts on $n + d$ nodal degrees of freedom only and we won't destroy this hierarchy information, as explained above, in order to construct an efficient preconditioner for crack growth problems. Thus, we introduce a restriction operator $\mathcal{R}$ of a fictitious space with $2n+2d$ nodal degrees of freedom onto our realistic space of $n+2d$ nodal degrees of freedom by means of:

$$\mathcal{R} = \begin{pmatrix} \frac{1}{2}I & \mathbb{O} & \frac{1}{2}I & \mathbb{O} \\ \mathbb{O} & I & \mathbb{O} & \mathbb{O} \\ \mathbb{O} & \mathbb{O} & \mathbb{O} & I \end{pmatrix}. \tag{3.5}$$

Finally, we guess the necessary resulting preconditioner in form of a two time C^{-1} - application regarding

$$\mathcal{R} \begin{pmatrix} C^{-1} & \mathbb{O} \\ \mathbb{O} & C^{-1} \end{pmatrix} \mathcal{R}^T. \tag{3.6}$$

This results in the following procedure:
Let $\underline{r} = \left(\underline{r}_0^T, \underline{r}_-^T, \underline{r}_+^T\right)^T$ be the residual vector in the k–th iteration of the conjugate gradient algorithm with the parts $\underline{r}_0, \underline{r}_-$ and $\underline{r}_+$ referring to usual, "–"-nodes and "+"-nodes, respectively. Then, the preconditioner has to produce the preconditioned residual $\underline{w}$ as

$$\underline{w} = \mathcal{R} \begin{pmatrix} C^{-1} & \mathbb{O} \\ \mathbb{O} & C^{-1} \end{pmatrix} \mathcal{R}^T \underline{r}, \tag{3.7}$$

[2] We write 'n usual nodal degrees of freedom' for the indication of two degrees of freedom per node

which contains two preconditioning calls:

$$\begin{pmatrix} \underline{w}_{0,-} \\ \underline{w}_{-} \end{pmatrix} := C^{-1} \begin{pmatrix} \frac{1}{2}\underline{r}_0 \\ \underline{r}_{-} \end{pmatrix} \tag{3.8}$$

and (after copying of $\underline{r}_+$ to the "–"-data)

$$\begin{pmatrix} \underline{w}_{0,+} \\ \underline{w}_{+} \end{pmatrix} := C^{-1} \begin{pmatrix} \frac{1}{2}\underline{r}_0 \\ \underline{r}_{+} \end{pmatrix}. \tag{3.9}$$

This calculates different values on the usual nodes, which are averaged for defining $\underline{w}$:

$$\underline{w} = \begin{pmatrix} \frac{1}{2}(\underline{w}_{0,+} + \underline{w}_{0,-}) \\ \underline{w}_{-} \\ \underline{w}_{+} \end{pmatrix}. \tag{3.10}$$

The two solvers in (3.8) and (3.9) are the cheapest hierarchical basis preconditioners acting on the nodal degrees of freedom, which are referenced from the edge data, keeping in mind the hierarchical data structure during crack propagation. Thus, they should produce an analogous efficient iteration behavior as presented in the previous chapter for a standing crack.

4 Interaction integral

Based on the crack advance criteria (2.12,2.13) or (2.14) and given Δa, quasi-static crack prolongation can be simulated by means of the numerical technique introduced in section 3. This way, the K-factors K_I and K_{II} must be determined at each load level. In general, it is not possible to extract K_I and K_{II} from the usual numerical near tip solution without taking into consideration the special asymptotic behavior in the solution procedure and in the postprocessing stage. This is the case as well, even though a very fine finite element net is reached after appropriate adaptive mesh refinement at the crack tip. Therefore, we will apply the J-integrals defined in section 2 for the numerical determination of the K-factors exploiting their path independence in order to execute the numerical calculations away from the tip. This is possible for a general curved crack propagation only, when Δa may be assumed as straight lines, whereby the so-called two-dimensional interaction integral technique [33] can be used.

The essential point of this approach consists in the fact that the integrals along the straight Δa - contours Γ^- and Γ^+ (Figure 2), which include the near tip field is excluded from numerical calculations. The method considers two states of the cracked region:

- State 1 ($\boldsymbol{\sigma}^{(1)}$, $\boldsymbol{\varepsilon}^{(1)}$, $\boldsymbol{u}^{(1)}$) represents the current FEM-solution for which the K-factors $K_I = K_I^{(1)}$ and $K_{II} = K_{II}^{(1)}$ has to be calculated at a given load level and crack length, and

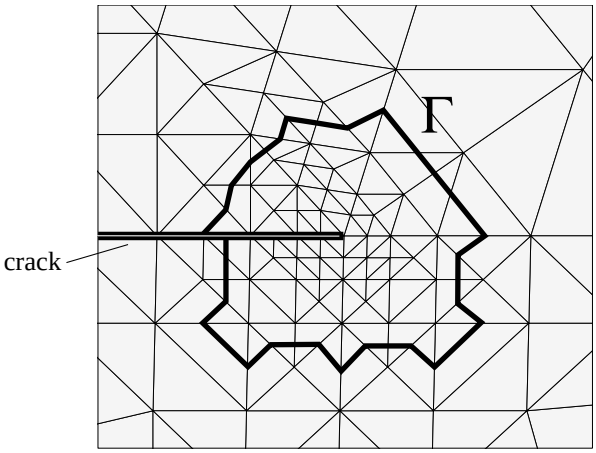

Figure 6: Finite element mesh with the J_x-integral contour Γ

- State 2 ($\boldsymbol{\sigma}^{(2)}$, $\boldsymbol{\varepsilon}^{(2)}$, $\boldsymbol{u}^{(2)}$) which is realized either by means of the full field Mode I eigenfunction [15] with the associated factor $K_I^{(2)}$ or by means of the full field Mode II eigenfunction [15] with the associated factor $K_{II}^{(2)}$.

The J_x-integral for the sum of these two states follows from (2.9) and (2.10) and the state definitions above in the form:

$$J_x^{(1+2_i)} = J_x^{(1)} + J_x^{(2_i)} + J_x^{(1*2_i)}, \quad i = I, II \tag{4.1}$$

with the notation

$$J_x^{(1*2_i)} = \int_\Gamma \left[(\boldsymbol{\sigma}^{(1)} : \boldsymbol{\varepsilon}^{(2_i)}) \boldsymbol{e}_x \cdot \boldsymbol{n} - \boldsymbol{e}_x \cdot (\boldsymbol{\nabla} \boldsymbol{u}^{(1)} \cdot \boldsymbol{\sigma}^{(2_i)} + \boldsymbol{\nabla} \boldsymbol{u}^{(2_i)} \cdot \boldsymbol{\sigma}^{(1)}) \cdot \boldsymbol{n} \right] ds, \quad i = I, II. \tag{4.2}$$

The index i in (4.1) and (4.2) denotes the use of the Mode I eigenfunction ($i = I$) or the Mode II eigenfunction ($i = II$) with respect to the state 2 respectively. Note on the one hand that the integration contour Γ does not contain any lines of the crack faces including the parts directly connected to the crack tip as shown in Figure 6 for an example net. This follows from the fact that only the J_x- components of the J- integral vector are used in the calculations. These components have no contributions from the straight crack faces Δa. On the other hand, Γ reaches the crack faces at a distance from the tip which must be less than $|\Delta a^+| = |\Delta a^-|$. The integrals $J_x^{(1*2_i)}$ are proportional to $K_I^{(2)}$ ($i = I$) and $K_{II}^{(2)}$ ($i = II$). On the other hand, the application of the superposition principle for the two states defined above to relation (2.11) results in the formulae:

$$J_x^{(1+2_I)} = J_x^{(1)} + J_x^{(2_I)} + \frac{2}{E^\star} \left(K_I^{(1)} K_I^{(2)} \right), \quad J_x^{(1+2_{II})} = J_x^{(1)} + J_x^{(2_{II})} + \frac{2}{E^\star} \left(K_{II}^{(1)} K_{II}^{(2)} \right) \tag{4.3}$$

with $E^\star = E/(1-\nu^2)$ (for plane strain). (4.1), (4.2) and (4.3) give the necessary relations for the K-factors:

$$K_I = K_I^{(1)} = \frac{E^\star}{2K_I^{(2)}} J_x^{(1*2_I)}, \quad K_{II} = K_{II}^{(1)} = \frac{E^\star}{2K_{II}^{(2)}} J_x^{(1*2_{II})} \tag{4.4}$$

Thus, the K-factors can be calculated numerically by means of (4.4) based on the numerical solution of the current load step and the corresponding singular eigenfunctions along Γ.

5 Numerical test examples of crack propagation

5.1 Crack propagation of a symmetrically loaded specimen

The first test example (Figure 7) represents the crack propagation simulation of a symmetrically loaded tension specimen (K_{Ic}=450MPa$\sqrt{\text{mm}}$, $|\Delta a^+|=|\Delta a^-|$=2.5mm, $E=2\cdot 10^5$MPa, ν=0.3). Figure 7 shows the geometry together with the initial mesh. Throughout the following, all geometrical descriptions are given in the length unit mm. The specimen is loaded by means of uniform displacements u=0.05mm at the left side of the specimen (Figure 7). The given load induces the crack propagation immediately and the crack propagates continuously up to its arrest. Figure 8 shows the adaptive refined meshes for different crack lengths. The numbers placed down right in the pictures represent the accumulated numbers of the realized PCGM-solutions up to the current reached crack length. The pictures indicate mesh refinement and mesh coarsening during crack growth. The mesh of the region surrounding the old crack tip is coarsened if a certain distance to the current crack tip is exceeded. The fourth picture in Figure 8 shows the final position of the crack tip for the given material properties and load conditions, i.e., the crack stops. In this context, the dependence of the stress intensity factor on the crack length a is given in Figure 9.

Because of the symmetric loading conditions with respect to the crack trajectory resulting in $\rho = 0$, the crack advance conditions (2.12) together with (2.13) coincide with the hoop

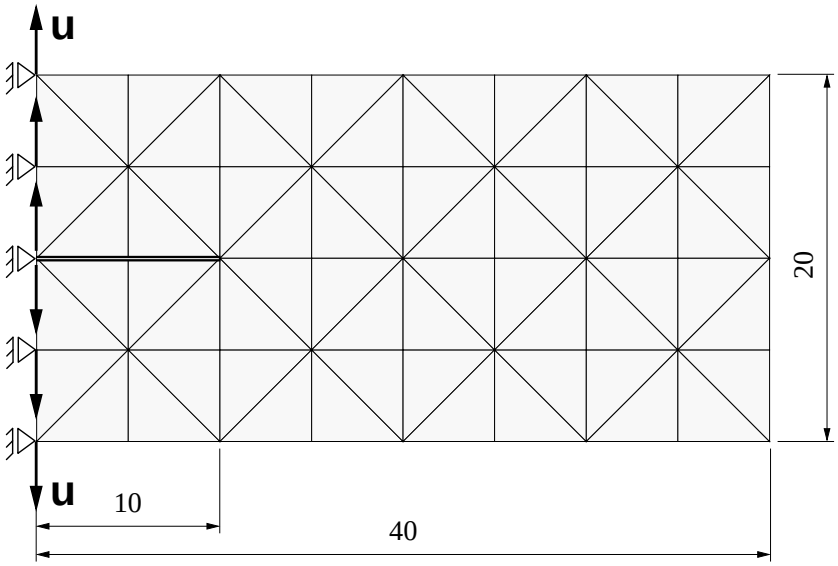

Figure 7: Symmetric tension specimen

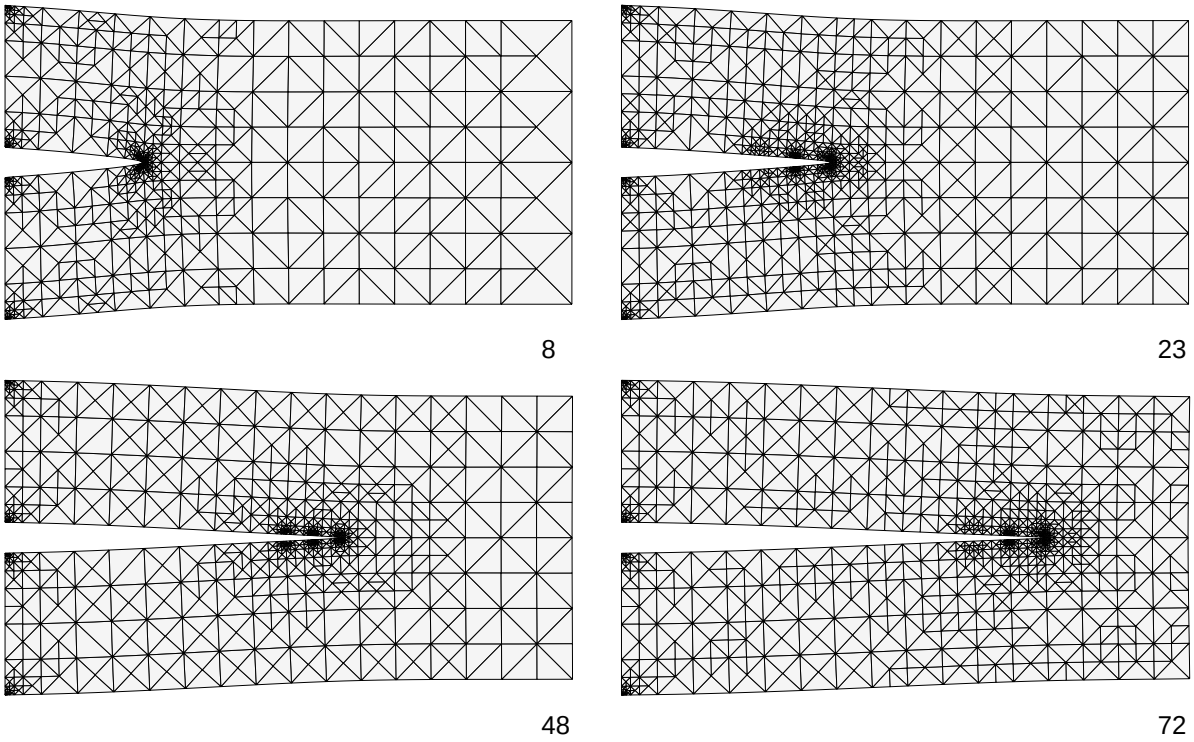

Figure 8: Crack propagation stages under symmetric loading

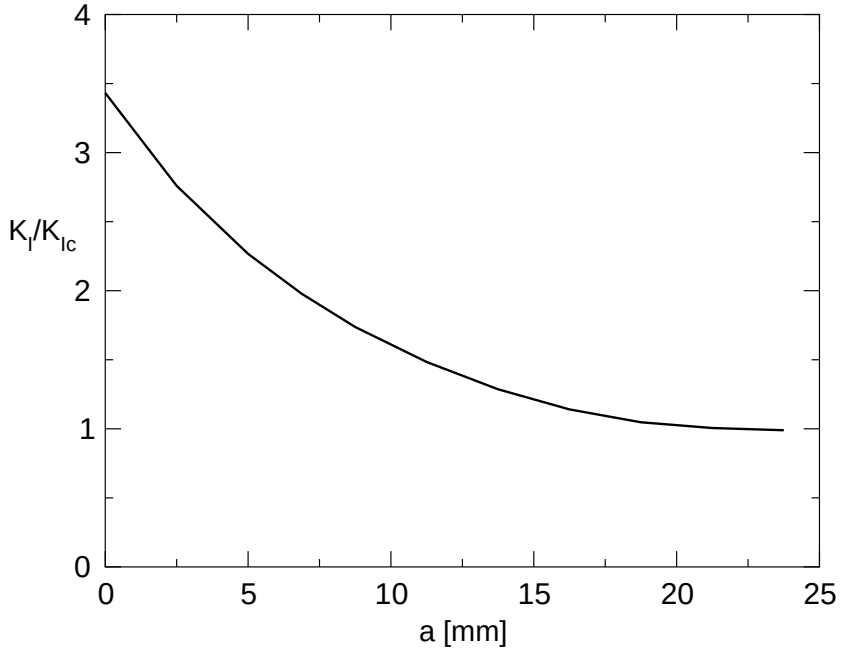

Figure 9: Change of the stress intensity Factor during crack propagation

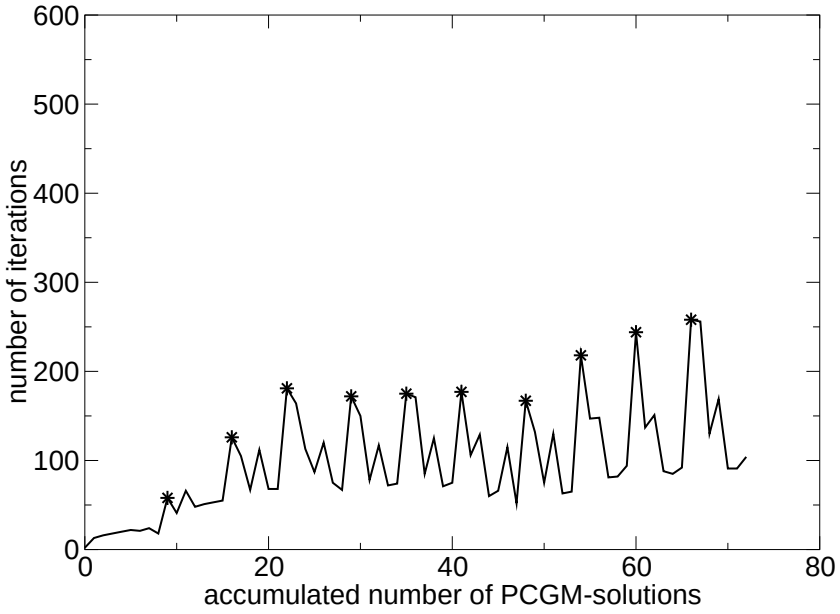

Figure 10: Iteration numbers of the PGCM-solver with respect to each realised

stress criteria (2.14). Thus, we get for both criteria the same crack propagation problems in this case.

Another interesting point follows from Figure 10, where the development of the iteration numbers for each PCGM-solution is diagrammed during the crack growth. The marked points indicate the solution directly after crack extension.

Obviously, the solver needs more iteration when the crack moves on and the mesh has to be corrected with respect to the new surfaces Δa. On the other hand, further mesh refinement leads to a rapid decrease of the iterations almost to their initial numbers. This circumstance expresses the high efficiency of the applied solution technique (section 3) and will be explained in a more remarkable sense analyzing the same problem with higher accuracy at the crack tip.

The accuracy of the solution at the crack tip can be characterized, besides the error estimator based on (3.1) to (3.4), exploiting the J-integral path independence. Thus, the mesh of the tip neighborhood should be refined up to the instant when the differences between the J-integrals calculated along three different contours Γ (the maximum of the differences related to the average value according to the values of $J_x^{(1*2_I)}$) are less than a given constant ϵ. In the calculations above, ϵ was chosen to be $\epsilon = 10^{-2}$. If one changes ϵ to $\epsilon = 10^{-3}$, the solution accuracy growths, i.e., the equation system contains more degrees of freedom and is more difficult to solve, but the results from Figure 10 change to those of Figure 11. Regardless the fact that the PCGM-iterations grow up to about 400 in the first solution step with the new surfaces Δa, the number of these iterations returns very rapidly to its initial values of less than 100. This way, the solution technique introduced in section 3 reaches very high efficiency for crack growth problems in fracture mechanics. In addition,

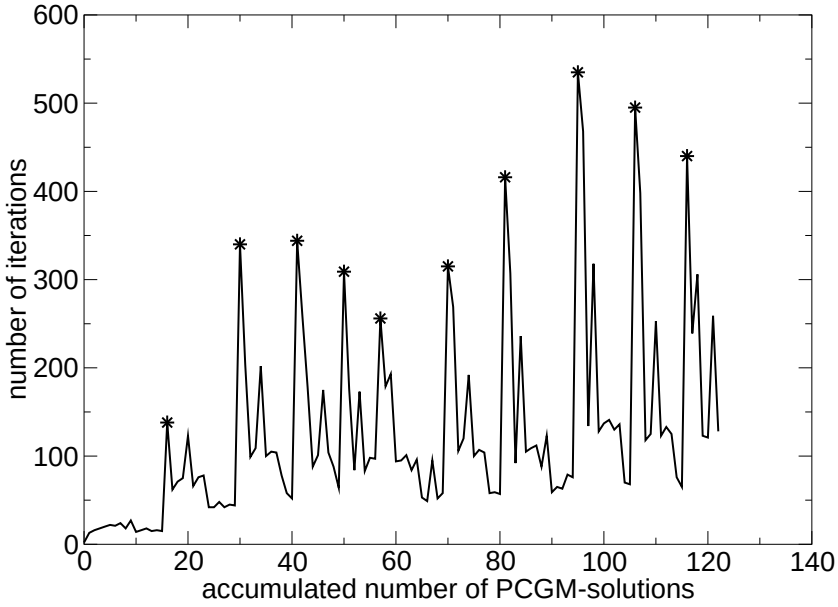

Figure 11: Iteration numbers of the PGCM-solver with respect to each realised solution for higher accuracy

it should noticed that the peak values in figures 10 and 11 have to be removed by further perfectioning of the developed numerical technique. The first step in this direction consists in the inclusion of the correct asymptotic solution behavior at the crack tip directly based on the research given in [29, 30, 31, 32]. This procedure will improve the condition number of the equation system to solve and, thus, reduce the PCGM-iterations.

5.2 Transverse force bending test

The second demonstration example represents the transverse force bending test used in the literature [36] simulating fatigue crack propagation. The specimen‘s geometry and the load conditions are shown in Figure 12 (K_{Ic}=1·MPa$\sqrt{\text{mm}}$, $|\Delta a^+|=|\Delta a^-|$=3mm, q=100N/mm). We will compare our numerical crack propagation simulation with the experimental results of [36]. The connection to the fatigue crack propagation considered there will be realized through the identification of K_{Ic} with the corresponding threshold value ΔK_{th} which is given small enough to have continuous crack growth.

Figure 13 shows the results of the simulation for different crack lengths in connection with the associated refined meshes. The numbers placed down right in the pictures again stand for the accumulated numbers of the realized PCGM-solutions. The crack advance conditions are based on the hoop stress criteria (2.14). The pictures indicate mesh refinement and mesh coarsening during crack growth. The mesh coarsening is mainly seen around the two holes. However, mesh coarsening occurs as well on the crack flanks shortly after the crack tip has left the corresponding crack surfaces. In contrast to the example in section

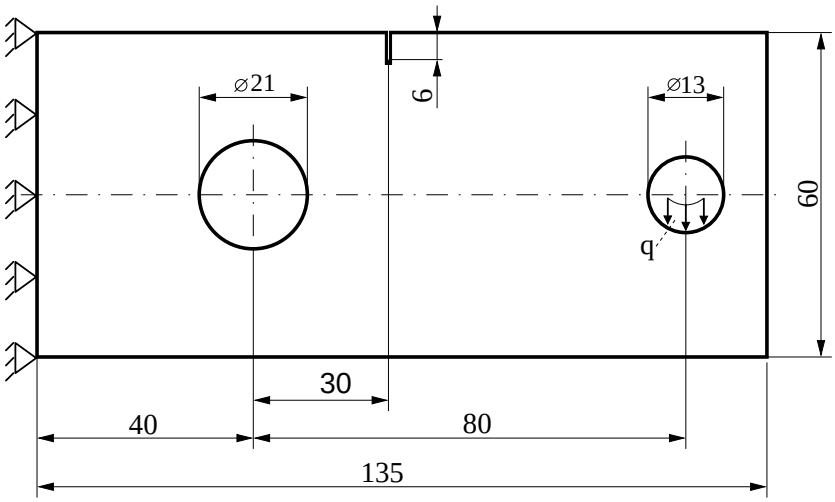

Figure 12: Transverse force bending test specimen

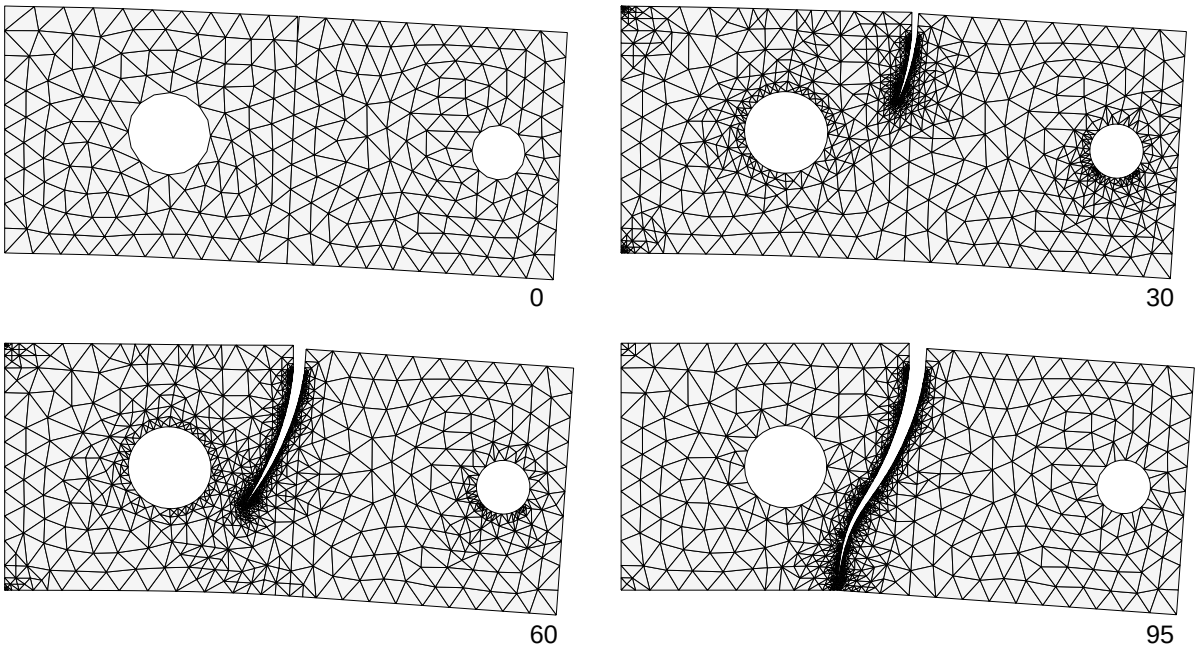

Figure 13: Simulation results for the transverse force bending test specimen

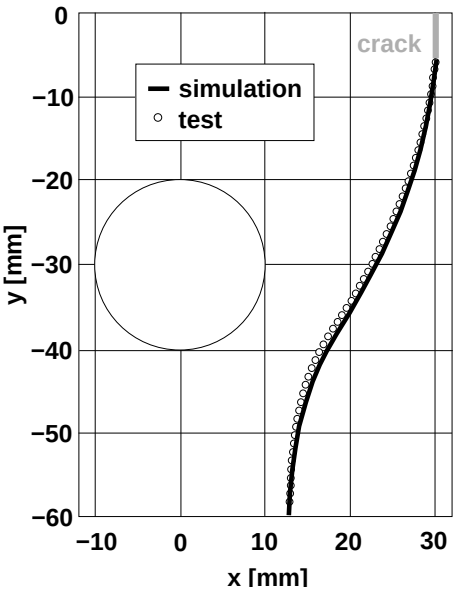

Figure 14: Comparison of the computed crack path with the experiment in [36]

5.1, new initial "father"-elements, which are smaller than the coarse elements of the symmetric crack arrest test, are produced during crack growth (see Figure 4). This is an effect of the fact that the crack does not propagate along element edges of the initial coarse mesh and results in the consequence that coarsening occurs up to the small "new crack growth initial father"-elements. Thus, one can find relative small elements along the surfaces of the propagating crack.

Figure 14 presents the comparison of the computed crack path with the realized experiment of [36]. The simulation shows a very good agreement. The small deviations are due to the overestimated crack advance parameter Δa. Finally, it should be mentioned that because of the small values ρ occurring during crack propagation, the application of the J-integral vector criteria (2.12, 2.13) instead of (2.14) leads with small differences to the same results shown above. Big differences between the two criteria appear for higher values of ρ. For instance, the loading conditions for the specimen shown in the left of Figure 15 lead to quite different crack paths given in the right of Figure 15.

6 Conclusions

Efficient solution techniques for the numerical simulation of crack propagation of 2D linear elastic formulations based on FEM together with the conjugate gradient method are developed. The numerical technique using hierarchical preconditioners comprehends the interesting feature that the hierarchical data structure will not be destroyed during crack propagation. Thus, one gets the possibility to simulate crack advance in a very effective numerical manner including adaptive mesh refinement and mesh coarsening. Although the PCGM-solver needs more iterations when the crack moves on and the mesh have to

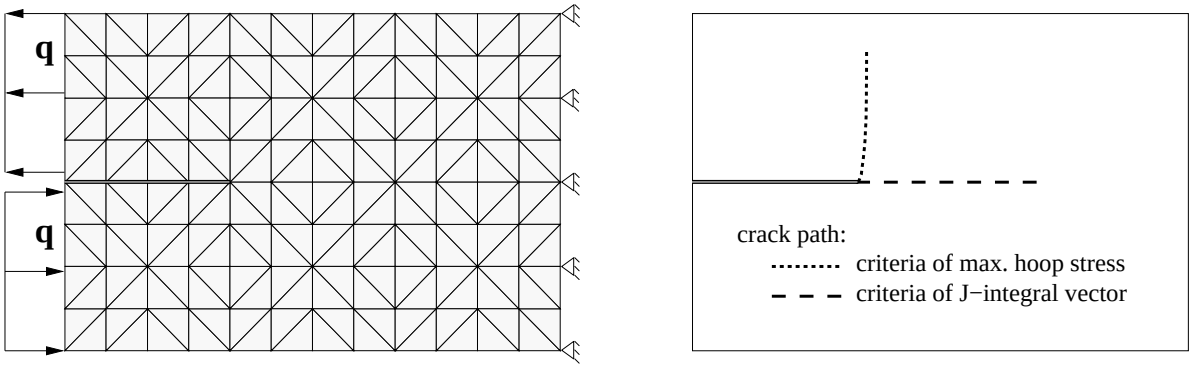

Figure 15: Model and results for shear loading

be corrected with respect to the new surfaces, further mesh refinement leads to a rapid decrease of the iterations almost to their initial numbers. The peak values of the PCGM-iterations should be removed by means of further approach perfectioning. The first step in this direction consists in the inclusion of the correct asymptotic solution at the crack tip directly. Test examples are presented to illustrate the efficiency of the given approach.

References

[1] M.H. Aliabadi: *Boundary element formulations in fracture mechanics.* Applied Mechanics Reviews 50(2), pp. 83–96, 1997.

[2] M.H. Aliabadi: *A new generation of boundary element methods in fracture.* International Journal of Fracture 86, pp. 91–125, 1997.

[3] E. Bänsch : *Local mesh refinement in 2 and 3 dimensions,* IMPACT of Computing in Science and Engineering 3 (1991), 181–191 .

[4] T. Belytschko and T. Black: *Elastic crack growth in finite elements with minimal remeshing.* International Journal for Numerical Methods in Engineering 45, pp. 601–620, 1999.

[5] T. Belytschko, N. Moës, S. Usui and C. Parimi: *Arbitrary discontinuities in finite elements.* International Journal for Numerical Methods in Engineering 50, pp. 993–1013, 2001.

[6] V.G. Boriskovsky and V.S. Parton: *Dynamic fracture mechanics (in Russian).* Progress in science and engineering, Mechanics of the deformable solid 16, pp. 1–78, 1983.

[7] I. H. Bramble, J. E. Pasciak and J. Xu : *Parallel Multilevel Preconditioners,* Math. Comp. **55** 191,(1990) 1-22.

[8] A. Carpinteri, G. Ferro and G. Ventura: *An augmented Lagrangian element-free (ALEF) approach for crack discontinuities.* Computer Methods in Applied Mechanics and Engineering 191, pp. 941–957, 2001.

[9] A. Carpinteri, G. Ferro and G. Ventura: *The partition of unity quadrature in meshless methods.* International Journal for Numerical Methods in Engineering 54, pp. 987–1006, 2002.

[10] G.P. Cherepanov: *Mechanics of Brittle Fracture.* McGraw-Hill, New York, 1979.

[11] D. Coker, A.J. Rosakis and A. Needleman: *Dynamic crack growth along a plymer composite-Homalit interface.* Journal of the Mechanics and Physics of Solids 51, pp. 425–460, 2003.

[12] Jacob Fish and Aditya Nath: *Adaptive and hierarchical modelling of fatigue crack propagation.* International Journal for Numerical Methods in Engineering 36, pp. 2825–2836, 1993.

[13] M. Fleming, Y.A. Chu, B. Moran and T. Belytschko: *Enriched Element-Free Galerkin methods for crack tip fields.* International Journal for Numerical Methods in Engineering 40, pp. 1483–1504, 1997.

[14] A. Gravouil, N. Moës and T. Belytschko: *Non-planar 3D crack growth by the extended finite element and level sets – Part II: Level set update.* International Journal for Numerical Methods in Engineering 53, pp. 2569–2586, 2002.

[15] D. Gross: *Bruchmechanik.* Springer–Verlag, Berlin–Heidelberg–New York, 1996.

[16] A. Huerta and S. Fernades-Mendes: *Enrichment and coupling of the finite element and meshless methods.* International Journal for Numerical Methods in Engineering 48, pp. 1615–1636, 2000.

[17] G.R. Irwin: *Analysis of stresses and strain near the end of a crack traversing a plate.* Transactions of the ASME, Journal of Applied Mechanics 24, pp. 361–364, 1957.

[18] S. Li and W.K. Liu: *Meshfree and particle methods and their applications.* Applied Mechanics Reviews 55(1), pp. 1–34, 2002.

[19] Shaofan Li and Wing Kam Liu: *Numerical simulations of strain localization in inelastic solids using mesh-free methods.* International Journal for Numerical Methods in Engineering 48, pp. 1285–1309, 2000.

[20] H. Liebowitz and E.T. Moyer: *Finite element methods in fracture mechanics.* Computers & Structures 31(1), pp. 1–9, 1989.

[21] W. K. Liu, S. Hao, T Belytschko, S. Li and C.T. Chang: *Multi-scale methods.* International Journal for Numerical Methods in Engineering 47(7), pp. 1343–1361, 2000.

[22] A. Meyer: *Hierarchical Preconditioners for Hihg Order Elements and Application in Computational Mechanics,* in: Developments in Computational Mechanics with High Performance Computing, B.Topping(edc.), Civil–Comp Press, Edinburgh 1999, S.107–112.

[23] N. Moës, A. Gravouil and T. Belytschko: *Non-planar 3D crack growth by the extended finite element and level sets – Part I: Mechanical model.* International Journal for Numerical Methods in Engineering 53, pp. 2549–2568, 2002.

[24] A. Needleman: *Numerical modeling of crack growth under dynamic loading conditions.* Computational Mechanics 19, pp. 463–469, 1997.

[25] T. Nishioka: *The state of the art in computational dynamic fracture mechanics.* JSME International Journal Series A 37(4), pp. 313–333, 1994.

[26] T. Nishioka: *Computational dynamic fracture mechanics.* International Journal of Fracture 86, pp. 127–159, 1997.

[27] J. Oliver, A.E. Huespe, M.D.G Pulido and E. Samaniego: *On strong discontinuity approach in finite deformation settings.* International Journal for Numerical Methods in Engineering 56, pp. 1051–182, 2003.

[28] Rolf Rannacher and Franz-Theo Suttmeier: *A feed-back approach to error control in finite element methods: Application to linear elasticity.* Reaktive Strömungen, Diffusion und Transport SFB 359, Interdiziplinäres Zentrum für Wissenschaftliches Rechnen der Universität Heidelberg, 1996.

[29] M. Scherzer: *Non-linear deformed interface corner stress characterization by effective parallel numerical methods.* In B.L. Karihaloo, Y.W. Mai, M.I. Ripley and R.O. Ritchie, Eds., Advances in Fracture Research, Proceedings of the 9th International Conference on Fracture 1-5 April 1997, Sydney, Australia, vol. 4, pp. 1959–1970, Amsterdam–Oxford–New York–Tokyo–Lausanne 1997. Pergamon Press.

[30] M. Scherzer: *Stress fields at interface-corners and cracks for non-linear deformations.* In H.-P. Rossmanith, Editor, Damage and Failure of Interfaces, Proceedings of the First International Conference – DFI-1/Vienna/Austria/22-24 September 1997, pp. 67–74, Rotterdamm/Brookfield 1997. A.A.Balkema.

[31] M. Scherzer: *Physikalisch und geometrisch nichtlineare Problemstellungen der Festkörper- und Bruchmechanik an Interface-Konfigurationen.* Habilitationsschrift, Technische Universität Bergakademie Freiberg 1999.

[32] M. Scherzer and A. Meyer: *Zur Berechnung von Spannungs- und Deformationsfeldern an Interface-Ecken im nichtlinearen Deformationsbereich auf Parallelrechnern.* Preprint-Reihe des Chemnitzer Sonderforschungsbereiches 393 (Numerische Simulation auf massiv parallelen Rechnern), Nr.: 96-03, TU Chemnitz-Zwickau, Fakultät für Mathematik, 1996.

[33] M. Stern, E.B. Becker and R.S. Dunham: *A contour integral computation of mixed-mode stress intensity factors.* International Journal of Fracture 12(3), pp. 359–368, 1976.

[34] T.J. Stone and I. Babuška: *A numerical method with a posteriori error estimation for determining the path taken by a propagating crack.* Computer Methods in Applied Mechanics and Engineering 160, pp. 245–271, 1998.

[35] A. Tabiei and J. Wu: *Development of the DYNA3D simulation code with automated fracture procedure for brick elements.* International Journal for Numerical Methods in Engineering 57, pp. 1979–2006, 2003.

[36] H. Theilig, M. Wünsche, and R. Bergmann: *Numerische und experimentelle Untersuchungen zur Entwicklung gekrümmter Ermüdungsrisse bei proportionaler zyklischer Belastung.* DVM-Bericht 235, pp. 239–248, Deutscher Verband für Materialforschung und -prüfung, Berlin, 2003.

[37] G. Ventura, J.X. Xu and T. Belytschko: *A vector level set method and new discontinuity approximation for crack growth by EGF.* International Journal for Numerical Methods in Engineering 54, pp. 923–944, 2002.

[38] P. Wriggers: *Nichtlineare Finite-Element-Methoden.* Springer, Berlin, 2001.

[39] H. Yserentant: *Two Preconditioners Based on the Multilevel Splitting of Finite Element Spaces,* Numer. Math. **58** (1990), 163-184.

Other titles in the SFB393 series:

03-01 E. Creusé, G. Kunert, S. Nicaise. A posteriory error estimation for the Stokes problem: Anisotropic and isotropic discretizations. January 2003.

03-02 S. I. Solov'ëv. Existence of the guided modes of an optical fiber. January 2003.

03-03 S. Beuchler. Wavelet preconditioners for the p-version of the FEM. February 2003.

03-04 S. Beuchler. Fast solvers for degenerated problems. February 2003.

03-05 A. Meyer. Stable calculation of the Jacobians for curved triangles. February 2003.

03-06 S. I. Solov'ëv. Eigenvibrations of a plate with elastically attached load. February 2003.

03-07 H. Harbrecht, R. Schneider. Wavelet based fast solution of boundary integral equations. February 2003.

03-08 S. I. Solov'ëv. Preconditioned iterative methods for monotone nonlinear eigenvalue problems. March 2003.

03-09 Th. Apel, N. Düvelmeyer. Transformation of hexahedral finite element meshes into tetrahedral meshes according to quality criteria. May 2003.

03-10 H. Harbrecht, R. Schneider. Biorthogonal wavelet bases for the boundary element method. April 2003.

03-11 T. Zhanlav. Some choices of moments of refinable function and applications. June 2003.

03-12 S. Beuchler. A Dirichlet-Dirichlet DD-pre-conditioner for p-FEM. June 2003.

03-13 Th. Apel, C. Pester. Clément-type interpolation on spherical domains - interpolation error estimates and application to a posteriori error estimation. July 2003.

03-14 S. Beuchler. Multi-level solver for degenerated problems with applications to p-version of the fem. *(Dissertation)* July 2003.

03-15 Th. Apel, S. Nicaise. The inf-sup condition for the Bernardi-Fortin-Raugel element on anisotropic meshes. September 2003.

03-16 G. Kunert, Z. Mghazli, S. Nicaise. A posteriori error estimation for a finite volume discretization on anisotropic meshes. September 2003.

03-17 B. Heinrich, K. Pönitz. Nitsche type mortaring for singularly perturbed reaction-diffusion problems. October 2003.

03-18 S. I. Solov'ëv. Vibrations of plates with masses. November 2003.

03-19 S. I. Solov'ëv. Preconditioned iterative methods for a class of nonlinear eigenvalue problems. November 2003.

03-20 M. Randrianarivony, G. Brunnett, R. Schneider. Tessellation and parametrization of trimmed surfaces. December 2003.